Interface controlled electrical and magnetic properties in Fe-Fe_3O_4–silica gel nanocomposites

D. Das, S. Roy, J. W. Chen, and D. Chakravorty

Citation: Journal of Applied Physics **91**, 4573 (2002); doi: 10.1063/1.1454197
View online: http://dx.doi.org/10.1063/1.1454197
View Table of Contents: http://aip.scitation.org/toc/jap/91/7
Published by the American Institute of Physics

Interface controlled electrical and magnetic properties in Fe–Fe_3O_4–silica gel nanocomposites

D. Das
Indian Association for the Cultivation of Science, Jadavpur, Calcutta 700 032, India

S. Roy[a] and J. W. Chen
Department of Physics, National Taiwan University, Taipei, 10617 Taiwan, Republic of China

D. Chakravorty[b]
Indian Association for the Cultivation of Science, Jadavpur, Calcutta 700 032, India

(Received 4 June 2001; accepted for publication 23 December 2001)

Iron nanoparticles with a shell of Fe_3O_4 phase with a total diameter of 5.3 nm have been grown within a silica gel matrix in the percolative configuration by suitable reduction followed by oxidation treatments. dc electrical resistivity measurements were carried out in the temperature range 80–300 K. The resistivity of the nanocomposites was found to be about 7 orders of magnitude lower than that of the reference gel. The electrical conduction has been explained on the basis of a small polaron hopping mechanism. The activation energy in the case of the composites was calculated from experimental data to be about one-fifth that for the reference sample. An interfacial amorphous phase is believed to cause such reduction in resistivity. The effective dielectric constant of this phase was estimated to be about four times that of the reference glass. Magnetization measurements on these specimens were carried out in the temperature range 5–300 K both in zero field cooled and field cooled states. A peak in the magnetization at ~120 K was ascribed to an order–disorder (Verwey) transition. Another peak at ~55 K was explained as arising due to a spin glass like disorder at the interface between the ferromagnetic iron ores and the ferrimagnetic Fe_3O_4 shell. A loop shift was observed as a result of the spin freezing below this temperature. © *2002 American Institute of Physics.* [DOI: 10.1063/1.1454197]

I. INTRODUCTION

Nanomaterials have occupied the center stage in physics research in recent times because of challenges thrown up by them both in theoretical understanding and practical applications.[1–7] Nanostructured materials have the characteristic feature of a large volume fraction of grain boundaries. Therefore the latter represent an ideal opportunity to study the structure and dynamics of thin films in confined geometries.[8] Molecular dynamics simulations of silicon grain boundaries have resulted in the conclusion that a confined amorphous equilibrium structure exists in those regions.[9,10] It is expected that in suitably engineered nanostructured materials it should be possible to observe physical properties different from that of their bulk counterparts. Recently, we have shown in nanocomposites comprising copper oxide within a silica gel the electrical conductivity arises due to the presence of an amorphous phase at the boundaries of the nanosized oxide layers.[11] The electrical conductivity was found to be about 6 orders of magnitude higher than that of the reference gel in which nanostructure was not developed. We have now been able to synthesize a silica gel with a microstructure such that nanoparticles of iron with a shell of Fe_3O_4 around them form a percolative path. Electrical resistivity is found to be orders of magnitude less than that of the precursor gel. The electrical properties are controlled by the interfacial amorphous phase. We have also carried out magnetic measurements on these samples over a wide temperature range. The magnetic behavior is controlled by the interfacial interaction between the ferromagnetic iron and ferrimagnetic Fe_3O_4 at around 50 K. The Verwey transition[12,13] at around 120 K is also exhibited by the nanoscale Fe_3O_4 phase. The details are reported in this article.

II. EXPERIMENT

The target gel composition for the preparation of the present set of samples was 55 Fe_2O_3, 45 SiO_2 (in mole %). The rationale behind the high percentage of Fe_2O_3 was to ensure that the gel after a reduction treatment produced a metallic percolation configuration. The precursors used were $FeCl_3$ and tetraethylorthosilicate. A solution was prepared by mixing 60 ml of ethyl alcohol, 10 ml of distilled water, and 23.174 g m of $FeCl_3$. This was stirred for 20 min. Another solution was made by mixing 90 ml of ethyl alcohol, 15 ml of distilled water, and 1 ml of HCl and stirring it for 20 min. The latter solution was added to 26.2 ml of tetraethylorthosilicate and the mixture stirred for 1 h. The first solution containing $FeCl_3$ was now added to the last one with tetraethylorthosilicate and the mixture was stirred for 1 h. The resultant sol was left undisturbed for 2 weeks for gelation. The gel was subjected to a reduction treatment in hydrogen at 923 K for 1/2 h. The gel powder was taken in a graphite

[a]On loan from Datar Switchgear Ltd., Nasik, India.
[b]Author to whom correspondence should be addressed; electronic mail: mlsdc@mahendra.iacs.res.in

mold with a diameter of 1 cm and then hot pressed at 923 K for 5 min by a sintering press DSP 25ATS manufactured by Dr. Fritsch Sondermaschinen GmbH. The mold chamber was evacuated to a pressure of $\sim 7.0\times10^{-3}$ Torr and the applied pressure was 2.4 MPa. Electrical measurement on the sample showed a metallic conduction indicating a percolation of the iron particles—the size of the latter was found from electron microscopic investigations to be on the order of 5.3 nm (see below). This is consistent with the results reported by us earlier in iron–silica nanocomposites.[14]

The gel powders reduced at 923 K for 1/2 h were subsequently heat treated in ordinary atmosphere at temperatures varying from 573 to 973 K for a duration of 1/2 h. This was done to generate an oxide layer on the iron nanoparticles. The resultant powders were hot pressed by the procedure described in the previous paragraph. For intercomparison of the electrical resistivity of different nanocomposites a reference sample was prepared by hot pressing the gel powder subjected to a heat treatment at 1123 K for 2 h in ordinary atmosphere.

The microstructure of different samples was investigated using a JEM 200 CX transmission electron microscope. Details of the specimen preparation have been described elsewhere.[15]

For measurement of dc resistivity the sample surfaces were first of all ground with 800 mesh size SiC powder. Two opposite faces of the sample were coated with silver paste supplied by Acheson Colloiden B. V. Holland. dc electrical resistances were measured by a 617 Keithley Electrometer over the temperature range 80–300 K under a vacuum of $\sim 10^{-2}$ Torr.

Magnetic measurements were carried out on different samples in the temperature range 5–300 K using a commercial superconducting quantum indifference device magnetometer with an applied magnetic field up to 12 kOe.

III. RESULTS AND DISCUSSION

Figure 1(a) is the transmission electron micrograph for a specimen subjected to a reduction treatment at 923 K for 1/2 h. Figure 1(b) is the electron diffraction pattern obtained from Fig. 1(a). Table I summarizes the values of interplanar spacings as obtained from the diameters of the diffraction rings. It is evident that the major phase present is α-Fe because the most intense diffraction peak is observed in our diffraction pattern viz., 0.203 nm. Some amount of Fe_3O_4 is also present. This arises due to a fast oxidation of the smaller iron particles in ordinary atmosphere. This has been found earlier also.[16] Figure 2(a) shows the transmission electron micrograph for a specimen obtained by hot pressing the gel powder first reduced at 923 K for 1/2 h followed by an oxidation treatment at 573 K for 1/2 h. Figure 2(b) is the corresponding electron diffraction pattern. In Table II the values of interplanar spacings estimated from the diffraction ring diameters are summarized and compared with standard ASTM data. It can be concluded from this table that Fe_3O_4 has grown around the iron nanoparticles in this specimen causing the appearance of most of its diffraction lines. This is typical of the other specimens subjected to different oxidation treatments. Figure 3 shows the particle size distribution in this specimen. The points represent the experimental data and the line the theoretical fit to a log-normal distribution function.[15] Such analysis was carried out for all the specimens. Table III summarizes the values of median diameter $\bar{x}$ and geometric standard deviation σ extracted by this analysis for the different samples. It is seen from this table that the median diameter deduced from electron micrographs decreases as the oxidation treatment of the gel powders is increased. This arises due to the formation of the Fe_3O_4 shell around the nanoparticles of iron as the oxidation treatment is

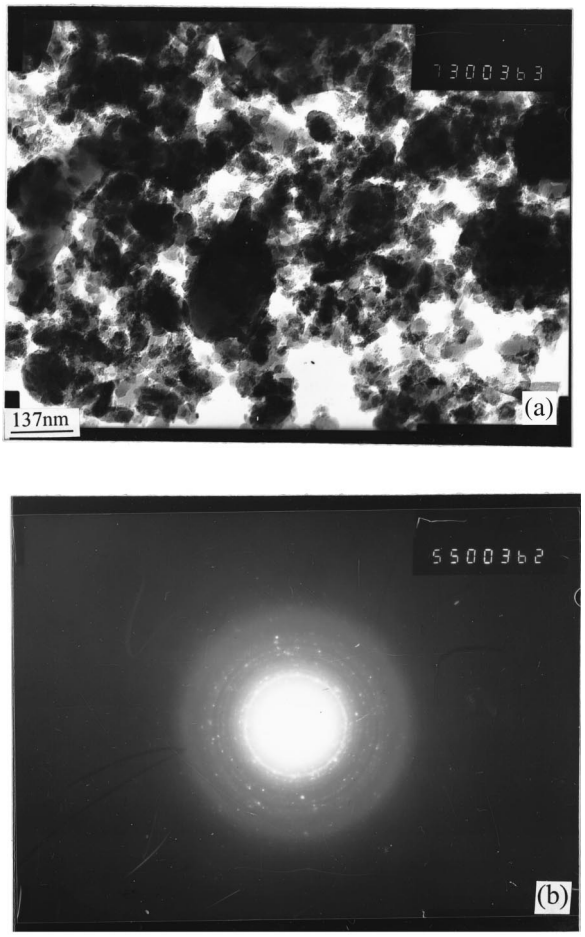

FIG. 1. (a) Transmission electron micrograph for specimen subjected to a reduction treatment at 923 K for 1/2 h. (b) Electron diffraction pattern obtained from (a).

TABLE I. Comparison of interplanar spacings d_{hkl} with standard ASTM data for specimen prepared by reduction of gel at 923 K for 1/2 h.

	ASTM	
Observed (nm)	α-Fe (nm)	Fe_3O_4 (nm)
0.203	0.202 68	
0.181		
0.162		0.1614
0.141	0.143 32	
0.129		0.1279
0.119	0.117 02	

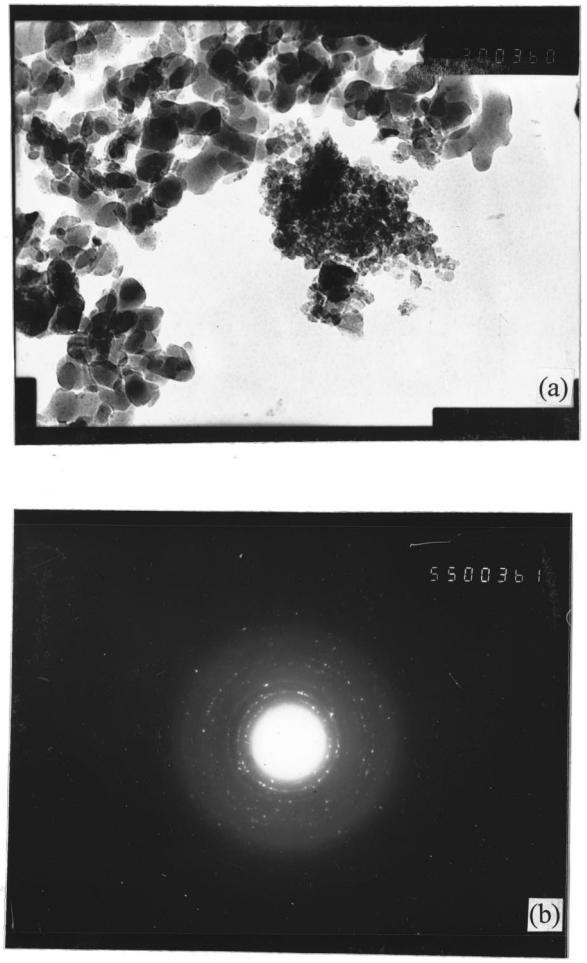

FIG. 2. (a) Transmission electron micrograph for specimen prepared by hot pressing of gel powder first reduced at 923 K for 1/2 h. followed by oxidation treatment at 573 K for 1/2 h. (b) Electron diffraction pattern obtained from (a).

enhanced. This in effect reduces the diameter of the iron core. The density of Fe_3O_4 is lower than that of Fe in the electron micrograph so we can observe only the iron particles.

Figure 4 shows the variation of dc electrical resistivity as a function of inverse temperature for different specimens. The resistivity variation with respect to temperature is also shown for the reference sample (gel) for comparison. It is evident that the resistivity for the reference gel-derived silica glass containing Fe_2O_3 is about 7 orders of magnitude higher

TABLE II. Comparison of interplanar spacings d_{hkl} with standard ASTM data for specimen prepared by hot pressing of gel powder reduced at 923 K/1/2 h following by oxidation treatment at 573 K/1/2 h.

	ASTM	
Observed (nm)	α-Fe (nm)	Fe_3O_4 (nm)
0.253		0.251
0.220	0.202 68	0.220
0.185		0.1838
0.139	0.1433	0.1349
0.129	0.1170	0.1310

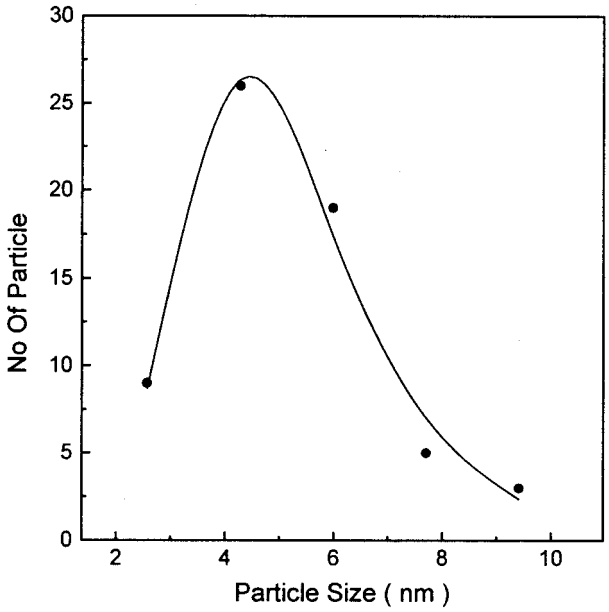

FIG. 3. Histogram of oxide-coated iron particles obtained from Fig. 2(a).

than that of the specimens in which the Fe–Fe_3O_4 core–shell nanostructure forms a percolative network. The latter conclusion is based on the fact that the oxide nanolayer was induced to a percolative configuration of metallic iron nanoparticles by subjecting them to an oxidation treatment. It has been shown earlier that dc conductivity in sol–gel derived glasses in the system Fe_2O_3–SiO_2 arises due to small polaron hopping between Fe^{2+} and Fe^{3+} sites.[17] The expression of resistivity in this model is given by[18]

$$\rho = \frac{kTR}{\nu_0 e^2 C(1-C)} \exp(2\alpha R) \exp(W/kT), \tag{1}$$

where ν_0 is the optical phonon frequency, α^{-1} the radius of wave function localization, R the average hopping distance, C the ratio of Fe^{2+} concentration to the total Fe ion concentration, k the Boltzmann constant, and W the activation energy. The latter is given by[19]

TABLE III. Median diameter $\bar{x}$ and geometric standard deviation σ for different samples as extracted by fitting to a log-normal distribution function.

Specimen No.	Heat treatment schedule for gelpowder before hot pressing	Median diameter $\bar{x}$ (nm)	Geometric Standard deviation σ
1	Reduced at 923 K/1/2 h	5.3	1.4
2	Reduced at 923 K/1/2 h +Oxidized at 573 K/1/2 h	4.9	1.4
3	Reduced at 923 K/1/2 h +Oxidized at 673 K/1/2 h	4.6	1.4
4	Reduced at 923 K/1/2 h +Oxidized at 773 K/1/2 h	4.4	1.4
5	Reduced at 923 K/1/2 h +Oxidized at 873 K/1/2 h	4.2	1.4
6	Reduced at 923 K/1/2 h +Oxidized at 973 K/1/2 h	4.1	1.4

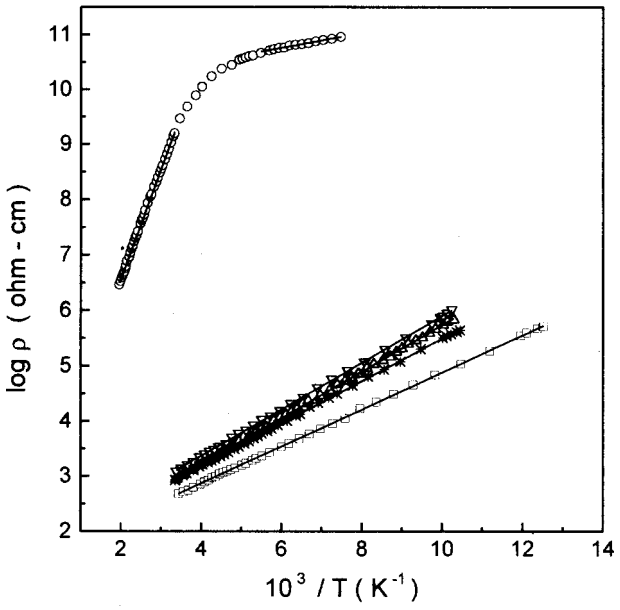

FIG. 4. Variation of dc electrical resistivity as a function of inverse temperature for different specimens: (○) reference sample, (○) specimen No. 2, (△) specimen No. 3, (*) specimen No. 4, and (□) specimen No. 5.

$$W = W_H + W_{D/2} \quad \text{for } T > \theta_{D/2}, \tag{2a}$$

$$W = W_D \quad \text{for } T < \theta_{D/4}, \tag{2b}$$

where W_H is the hopping energy, W_D the disorder energy, and θ_D the Debye temperature. W_H represents the Coulombic energy needed by the electron at the localized state of the transition metal (TM) ion to overcome the barrier to hop to the nearest localized state. W_D the disorder enerty arises due to the variation of local arrangements of the TM ions.

The high temperature portion of the resistivity temperature variation in the case of reference sample was fitted to Eq. (1) using C, α, R, and ν_o as parameters. The activation energy W was calculated from the slopes of $\log \rho$ versus lT plots. The least square fit is shown by the solid line in Fig. 4 and the extracted parameters are given in Table IV. The value of θ_D is given by $\theta_D = h^{\nu_0}/k$. Using the value of ν_0 extracted from the least square fitting we calculate a value of $\theta_D = 577$ K. This is consistent with the fact that a constant slope has been obtained at temperatures higher than $\theta_D/2$ i.e., 289 K in the case of reference sample. We have fitted the low temperature data of the latter by Eq. (1) and obtain the values $C = 0.999$, $\alpha = 0.89$, $R = 13.3$ Å, and $W = 0.03$ eV. Evidently, the latter is the disorder energy, because the slope pertains to data for temperatures lower than $\theta_D/4$, i.e., 144 K. A large value of R in this temperature range is consistent with the variable range hopping conduction mechanism.

TABLE IV. Parameters extracted by fitting resistivity data of $Fe–Fe_3O_4–SiO_2$ gel nanocomposites to Mott's model.

Specimen No.	W (eV)	α ($Å^{-1}$)	R (Å)	C	ν_0 (s^{-1})
Reference	0.39	0.95	4.7	0.99	1.2×10^{13}
2	0.08	0.89	4.7	0.99	1.3×10^{13}
3	0.08	0.86	4.8	0.99	1.2×10^{13}
4	0.07	0.87	4.9	0.99	1.1×10^{13}
5	0.06	0.86	4.8	0.99	1.3×10^{13}

The experimental data for specimens 2, 3, 4, and 5 were also fitted to Eq. (1) using C, α, R, ν_0 and W as parameters. The fitted curves are shown as solid lines in Fig. 4 and the extracted parameters are listed in Table IV. It is seen that the value of C for all specimens (including the reference sample) is rather large viz., close to unity. This means in all these specimens the major portion of iron ions has a valency state Fe^{2+}. This is because the electrical measurements were carried out under vacuum in which case the fraction of lower valence iron ions would increase. The value of α for all specimens is near unity, which is to be expected for small polaron hopping conduction. The activation energy for hopping in the case of reference sample is 0.39 eV, whereas for the different nanocomposites the value is much less viz., almost 1/5 that of the reference sample. The value decreases as the Fe_3O_4 shell thickness is increased. The trend of data obtained therefore indicates that the interfaces between the nanoscale shells of Fe_3O_4 constitute an amorphous phase different from that of the precursor gel-derived glass. It should be mentioned here that we have checked the possibility of the Fe_3O_4 shell contributing to the conduction process of the nanocomposites. It is known that Fe_3O_4 exhibits a sharp change of electrical resistivity by nearly 2 orders of magnitude at around 120 K.[12,13] This has been ascribed to an order–disorder transformation of the cations on the octahedral sites. In the present set of samples, magnetic measurements at low temperatures (see below) do indeed show the presence of this transformation. However, our electrical resistivity data do not exhibit any such change. The effect of the Fe_3O_4 layer on the measured electrical resistivity of the present set of nanocomposites has therefore been ruled out.

We have considered another possibility of electrical conduction in the present case. The metal particles with their oxide layers around them could contribute to electrical transport by an electron tunneling mechanism. The activation energy for such tunneling is given by[20]

$$\phi = \frac{1.44}{\varepsilon}\left[\frac{1}{r} - \frac{1}{r+s}\right]\text{eV}, \tag{3}$$

where r and s are the radius of the metallic grain and the separation between grains, respectively, expressed in nanometers and ε is the dielectric constant of the intervening medium. Taking $r = 2.45$ nm, $s = 5.30$ nm (data from Table III for specimen No. 2), and $\varepsilon \sim 14.2$ (for Fe_3O_4)[21] an activation energy $\phi = 0.027$ eV is calculated. This is much smaller than the experimentally determined activation energy from the slope of $\log \rho$ versus $1/T$ plot viz., 0.08 eV. Such discrepancies were found between the estimated and experimental values for other specimens also in the case of the electron tunneling mechanism.

We have also explored the possibility of the simultaneous presence of some percolating clusters of metallic iron and iron particles separated by Fe_3O_4 layers. As reported earlier such a configuration leads to a variation of $\log \rho$ as a function of T^{-1}, which shows a maximum at around 200 K.[22] No such feature was observed in the present set of data.

TABLE V. Estimated effective dielectric constant for interfacial amorphous phase in different nanocomposites.

Specimen No.	ε_p [calculated from Eq. (3)]
Reference	4.9
2	23.8
3	23.3
4	26.1
5	31.1

On the basis of the above discussion we rule out the effect of any electron tunneling contribution or a combination of percolating metallic chain and electron tunneling mechanism.

To get some insight into the nature of the interfacial amorphous phase we estimate the effective dielectric constant of this phase by the following procedure. According to the Austin–Mott model the activation energy W is approximately equal to half the polaron hopping energy.[19] We can then write

$$W = e^2/4\varepsilon_p r_p, \tag{4}$$

where ε_p is the effective dielectric constant and r_p the polaron radius. The latter can be written as[19]

$$r_p = \left(\frac{R}{2}\right)(\pi/6)^{1/3}. \tag{5}$$

We estimated r_p from Eq. (4) using the R values deduced from a previous analysis. Thereafter from Eq. (3) using the experimental W values we calculated the values of ε_p for different specimens. We summarize the values of the effective dielectric constant ε_p as deduced by this method in Table V. It is evident that the interfacial amorphous phase has a much larger dielectric constant than the precursor silica glass phase. This is consistent with the results reported earlier involving nanophase copper oxide interfaces.[11] The increase in ε_p is however more drastic in the present series of samples. The amorphous phase envisaged here consists largely of Fe_3O_4, which has a dielectric constant of $\sim$14.2. It appears therefore that the effective dielectric constant is around 60% higher in this interfacial phase. It is likely that the growth of Fe_3O_4 by oxidation of percolating iron particles will subject the Fe_3O_4 layers to a high pressure. The effect of high pressure on the dielectric properties of glasses is known.[23] It appears therefore that a high density interfacial amorphous phase has been generated in the samples. However, this needs to be substantiated by other characterization techniques like x-ray photoelectron spectroscopy and Mossbauer spectroscopy.

Figure 5 shows the variation of magnetization as a function of temperature in both field-cooled (FC) and zero FC (ZFC) states, respectively, for specimen No. 5. The specimen was FC at a magnetic field of 1 kOe. It is evident both the ZFC and FC data show a peak at around 120 K. This had been reported earlier as arising out of an order–disorder transformation.[12,13] More specifically below this transition temperature the cations on the octahedral sites start getting ordered, thus bringing about a lowering of the magnetization. As discussed earlier this transition has not shown any effect on the electrical resistivity behavior in the present set of specimens.

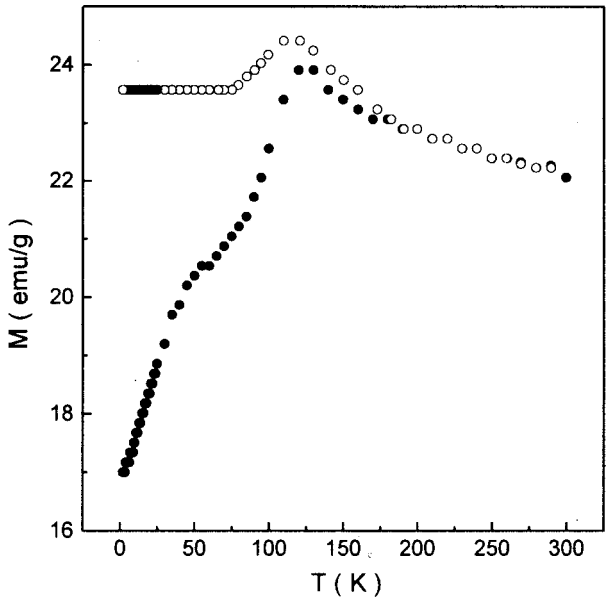

FIG. 5. Variation of magnetization for specimen No. 4 in ZFC and FC states as a function of temperature: (●) ZFC; and (○) FC.

The ZFC curve in Fig. 5 also shows a hump at around 55 K indicating a peak in the magnetization value near that temperature. The FC data in this temperature range show a constant value. Also, the FC specimen shows a loop shift at temperatures below 100 K. This is given in Fig. 6 for specimen No. 5. It has been discussed earlier[20] that due to an exchange interaction between the ferromagnetic core of the nanometer-sized iron particles and the oxide surface with spin glass-like magnetic disorder below a certain

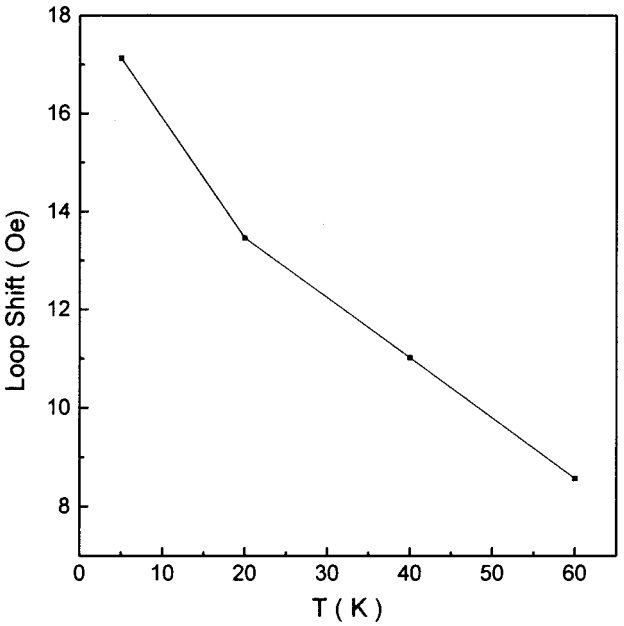

FIG. 6. Variation of loop shift as a function of temperature for specimen No. 5.

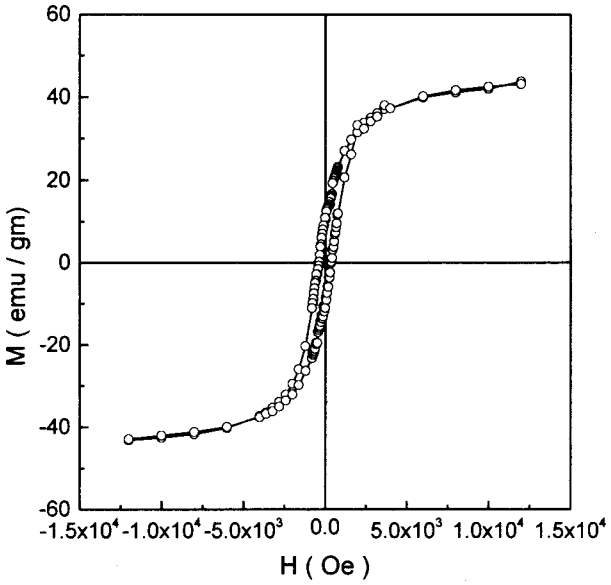

FIG. 7. Magnetic hysteresis loop for specimen No. 3 at 20 K.

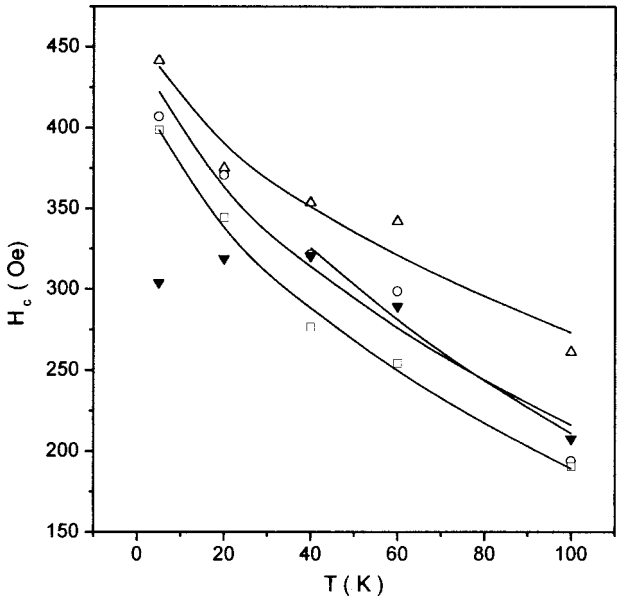

FIG. 8. Variation of coercivity H_C for different specimens as a function of temperature.

temperature—in this case around 55 K—the surface spins are frozen and these favor the ferromagnetic (iron) core of the composite particle being magnetized in the field cooling direction. This leads to a loop shift as observed in the present investigation. It should be noted that the magnitude of the loop shift is lower than that reported in the case of nanocomposites prepared by the electrodeposition method.[16] The Fe_3O_4 layer in the present study was prepared by a controlled oxidation treatment at a fairly high temperature, whereas in the earlier study the layer formed at the ambient temperature due to the reactive nature of the ultrafine iron particles. Therefore in the present system the iron core diameters are quite small and the effect of spin glass order at the interface between ferro- and ferrimagnetic phases on the extent of loop shift has also been found to be small. This is confirmed by our observation that the magnitude of loop shift becomes smaller in specimens subjected to higher oxidation treatments. The above results are typical of all the specimens studied here. It is to be noted that the FC and ZFC curves overlap at a temperature ~213 K. This is thus the blocking temperature T_B. From the data of specimen 4 we estimate a blocking temperature of 300 K. From the expression of T_B we get[23]

$$T_B = \frac{K'V}{25k}, \tag{6}$$

where K' is the effective anisotropy constant, V the volume of the ferromagnetic particle, and k the Boltzman constant. The ratio of the T_B for the above two specimens is 1.2. This is in satisfactory agreement with the ratio of the cubes of the particle diameters of the specimens concerned viz., 1.2.

Figure 7 is a typical hysteresis loop (M versus H) for specimen No. 3 taken under the ZFC condition at 20 K. The coercivity is seen to ~370 Oe. It is evident that the value is much higher than that of bulk iron. Such an increase is ascribed to the nanometer size of the iron particles.[16] In Fig. 8 is shown the variation of coercivity as a function of temperature for different specimens. It is seen that the coercivity value increases as the temperature is lowered. The theoretical expression for the temperature dependence of coercivity H_C for nanosized ferromagnetic particles is given by[23]

$$H_C = H_{CO}[1-(T/T_B)^{1/2}], \tag{7}$$

where H_{CO} is the coercive force at $T=0$ K, T the temperature of measurement, and T_B the blocking temperature above which superparamagnetism sets in. We have least square fitted the experimental data at different temperatures to Eq. (6) using H_{CO} and T_B as parameters. The solid lines are the theoretical fits and the points represent the experimental data. In Table VI the extracted parameters are summarized for different specimens. The decrease in T_B as the oxidation treatment of the iron particles is increased is consistent with the fact that such treatment reduces the diameter of the iron core. It should be noted that the coercivity shows a maximum at around 40 K for specimen No. 5. The iron core diameter is the least in this specimen. No satisfactory explanation is available at this stage for this behavior.

In summary, we have grown composites of iron core with a Fe_3O_4 shell of nanometer dimensions by suitable reduction and heat treatments in a silica gel matrix. The resistivity of the nanocomposite was found to be about 7 orders of magnitude lower than that of the reference gel. This is ascribed to the presence of an interfacial amorphous phase between the Fe_3O_4 shells. Magnetization measurements over

TABLE VI. Extracted values of H_{CO} and T_B for different specimens.

Specimen No.	H_{CO} (Oe)	T_B (K)
2	485	522
3	482	328
4	458	289
5	522	281

a wide temperature range showed an order–disorder transition at ~120 K. Another magnetization peak at around 55 K was explained as arising due to a spin glass-like disorder at the interface between the ferromagnetic iron core and the ferrimagnetic Fe_3O_4 shell.[24]

ACKNOWLEDGMENTS

D.C. acknowledges support by the Department of Science and Technology, the Government of India. J.W.C. acknowledges support through research Grant No. NSC 88-2111-M-002-021 by the National Science Council, Republic of China.

[1] J. R. Heath, Science **270**, 1315 (1995).
[2] A. P. Alivisatos, Science **271**, 933 (1996).
[3] R. P. Andres, J. D. Bielefeld, J. I. Henderson, D. B. Janes, V. R. Kolagunta, C. P. Kubiak, W. J. Mahoney, and R. G. Osifchin, Science **273**, 1690 (1996).
[4] Y. Imry, in *Nanostructures and Mesoscopic Systems*, edited by W. P. Kirk and M. A. Reed (Academic, New York, 1992), p. 11.
[5] A. J. Cox, J. G. Louderback and L. A. Bloomfield, Phys. Rev. Lett. **71**, 923 (1993).
[6] Y. M. Lin, S. B. Cronin, J. Y. Ying, M. S. Dresselhaus, and J. P. Jeremans, Appl. Phys. Lett. **76**, 3944 (2000).
[7] M. S. Fuhrer, J. Nygard, L. Shih, M. Forero, Y.-G. Yoon, M. S. C. Mazzoni, H. J. Choi, J. Ihm, S. G. Louie, A. Zettl, and P. L. McEuen, Science **288**, 494 (2000).
[8] H. Konrad, C. Karmonik, J. Weissmuller, H. Gleiter, R. Birringer, and R. Hempelmann, Physica B **234–236**, 173 (1997).
[9] P. Keblinski, S. R. Phillpot, D. Wolf, and H. Gleiter, Phys. Rev. Lett. **77**, 2965 (1996).
[10] P. Keblinski, D. Wolf, S. R. Phillpot, and H. Gleiter, Philos. Mag. Lett. **76**, 143 (1997).
[11] D. Das and D. Chakravorty, Appl. Phys. Lett. **76**, 1273 (2000).
[12] E. J. W. Verwey and P. W. Haayman, Physica (Utrecht) **8**, 979 (1941).
[13] E. J. W. Verwey, P. W. Haayman, and F. C. Rommeijn, J. Chem. Phys. **15**, 181 (1947).
[14] A. Chatterjee and D. Chakravorty, J. Mater. Sci. **27**, 4115 (1992).
[15] A. K. Maity, D. Nath, and D. Chakravorty, J. Phys.: Condens. Matter **8**, 5717 (1995).
[16] S. Banerjee, S. Roy, J. W. Chen, and D. Chakravorty, J. Magn. Magn. Mater. **219**, 45 (2000).
[17] P. Brahma, S. Mitra, and D. Chakravorty, Eur. J. Solid State Inorg. Chem. **28**, 1139 (1991).
[18] N. F. Mott, J. Non-Cryst. Solids **1**, 1 (1969).
[19] I. G. Austin and N. F. Mott, Adv. Phys. **18**, 41 (1969).
[20] C. A. Neugebauer and M. B. Webb, J. Appl. Phys. **33**, 74 (1962).
[21] *Handbook of Chemistry and Physics* (Chemical Rubber, Cleveland, OH, 1962), p. 2621.
[22] S. Banerjee and D. Chakravorty, J. Appl. Phys. **85**, 3623 (1999).
[23] D. Chakravorty and L. E. Cross, J. Am. Ceram. Soc. **47**, 370 (1964).
[24] E. H. Frei, S. Shtrikman, and D. Treves, Phys. Rev. **106**, 446 (1957).